# RSC Advances

ROYAL SOCIETY
OF CHEMISTRY

www.rsc.org/advances

# Table of Contents
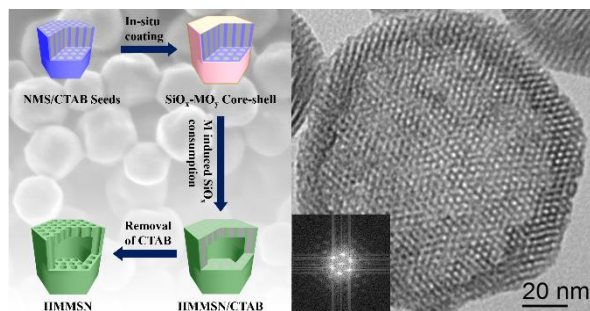


Monodispersed heteroatom-doped hollow nanocages with MCM-41 structures are synthesized by reacting nanosized MCM-41 seeds with in situ coated heteroatomic species.

# Journal Name

## COMMUNICATION

# Formation of uniform hollow nanocages with heteroatom-doped MCM-41 structures

Jiazhi Chen,[a,b] Fang Lu[*a] and Jie Xu[*a]

**Monodispersed Al, Sn, Fe, Nb, Ti -doped hollow nanocages (approx. 120 nm) with MCM-41 molecular sieve structures was synthesized by reacting nanosized MCM-41 silica seeds with in situ coated heteroatomic species. The Al-doped hollow MCM-41 nanocages have significantly improved accessible acid sites, which show enhanced activity in catalytic hydrolysis of cellobiose.**

Mesoporous silica materials are important in many areas because of their excellent properties, such as big pore size and high surface area.[1,2] Among them, MCM-41 molecular sieve shows unique features including highly ordered 2D hexagonal mesoporous structure and ultrahigh surface area.[3,4] It opens their broad utilizations in catalysis, adsorption, separation and biomedicine.[5-7] Pure MCM-41 materials have an electrically neutral framework.[8] The incorporation of trivalent or tetravalent ions, such as Al, Fe, Ti and Sn, into MCM-41 can further functionalize its properties, and create various acid and catalytic active sites.[9-12] Normally, heteroatom-doped MCM-41 presents in micrometer size which would make the diffusion of reactants ineffective, especially for large molecules. Therefore, it is essential to improve the accessibility of 2D hexagonal channels.

Recently, various materials with short MCM-41 channel length have been developed.[13-16] MCM-41 with hollow voids divides the microtubules into several interconnected nanotubules and builds tubule-within-tubule (TWT) hierarchical structures.[17] Nanosized MCM-41 particles provide mesoporous channels with hundreds of nanometers in length, which have additional properties of fast mass transfer and good suspension in solution.[18,19] Hollow-structured mesoporous silica nanoparticles (HMSNs), which integrate the hollow interiors and mesoporous shells, provide even shorter channel length with dozens of nanometers in the shells, and low density.[20,21] Only few literatures have been reported to change the surface electron characteristics by synthesizing heteroatom-doped HMSNs.[22-26] Fang et al[22] synthesized aluminum-doped HMSNs with perpendicular pore channel length in 40 nm. Interestingly, Li et al[23] prepared aluminum-doped HMSNs with MCM-48 molecular sieve structure (average size of the particle is approx. 600 nm, 70 nm in shell thickness) in 2003, and this material exhibits high hydrothermal stability. Since then, there has been no report on

synthesis of heteroatom-doped HMSNs with molecular sieve structure, because it is difficult to control the hydrolysis rate of heteroatom precursor to match that of silicon precursor, meanwhile maintaining the nanosized molecular sieve structure.

Herein, we report the synthesis of heteroatom-doped hollow nanocages with MCM-41 molecular sieve structures, average cage size of approx. 120 nm and shell thickness of 16 nm. The preparation of aluminum-doped hollow MCM-41 nanocage (HMASN) will be first demonstrated as an example, followed by more metallic elements, such as Sn, Fe, Nb, Ti. Monodispersed MCM-41 nanoparticles are first prepared by our previous reported process[19]. Then, these particles are employed as the seeds and in situ coated with a layer of heteroatomic species. The morphology of the core-shell structure subsequently changes from solid to hollow. The obtained HMASN was used as catalyst for the model reaction of cellobiose hydrolysis.
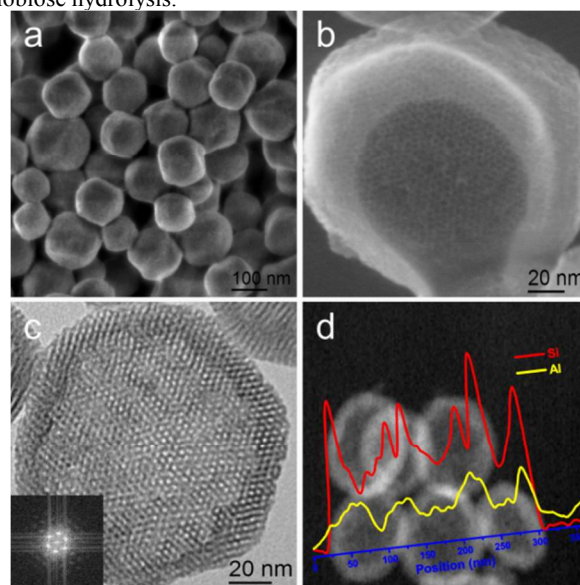


**Fig. 1** (a) SEM image of HMASN, (b) STEM image of a partially crushed HMASN, (c) TEM image of HMASN (the inset: FFT of the entire hexagonal core part in the image), (d) HAADF image of calcined HMASN and EDX line scan profiles.

COMMUNICATION

Fig. 1a shows a representative scanning electron microscope (SEM) image of uniform HMASN with average particle size of about 120 nm (Fig. S1a, b). Dynamic light scattering (DLS) demonstrates that the average hydrodynamic diameter of HMASN is also around 120 nm (Fig. S1c). The monodispersed HMASN displays a stable suspension in water (Fig. S1d). The scanning transmission electron microscope (STEM) image clearly shows the hollow morphology in HMASN (Fig. 1b). The high magnification transmission electron microscope (TEM) image demonstrates that HMASN possesses nearly hexagonal hollow structures. Meanwhile, the shells contain hexagonally arrayed mesopores and the shell thickness is around 16 nm (Fig. 1c and the inset). Moreover, the X-ray diffraction (XRD) pattern of HMASN exhibits typical peaks of p6mm 2D hexagonal symmetry including (100), (110), and (200) planes, which is in good agreement with the mesostructure of MCM-41 (Fig. S2). The energy dispersive X-ray (EDX) line scanning analysis across the hollow nanostructures reveals that the Si and Al contents are evenly distributed in the mesoporous shells (Fig. 1d). To investigate the incorporation of aluminum in silica, solid state $^{29}Si$ and $^{27}Al$ nuclear magnetic resonance (NMR) were performed (Fig. S3). HMASN has $Q^2$ $[(SiO)_2Si(OH)_2]$, $Q^3$ $[(SiO)_3SiOH]$, and $Q^4$ $[(SiO)_3SiOAl]$ siloxane units from $^{29}Si$ signals centered at -92, -101, and -108 ppm, respectively. $^{27}Al$ NMR spectrum shows that there are tetrahedrally coordinated aluminum atoms from the $^{27}Al$ signal at 53 ppm. It indicates that the aluminum is incorporated into the silica framework.

**Table 1** The textual parameters and acidic properties of several molecular sieves.

| Samples | Si/Al[a] | $S_{BET}$ ($m^2 g^{-1}$) | $V_P^{b}$ ($cm^3 g^{-1}$) | $D_P^{c}$ (Å) | $B^{d}$ (µmol $g^{-1}$) | $AB^{e}$ (µmol $g^{-1}$) |
|---|---|---|---|---|---|---|
| MSN | -- | 1329 | 2.0 | 25 | nd | nd |
| HMASN | 18 | 1291 | 3.9 | 25 | 59 | 57 |
| Al-MCM-41 | 19 | 1245 | 1.6 | 25 | 45 | 42 |
| HZSM-5 | 22 | 477 | 0.4 | 5.6[f] | 248 | 34 |

[a] Si/Al ratio obtained by using ICP. [b] The total pore volume measured at P/Po = 0.99. [c] The pore diameter calculated from the adsorption isotherm by the BJH method. [d] The amount of Brønsted acid sites calculated from FT-IR of adsorbed pyridine. [e] The amount of accessible Brønsted acid sites calculated from FT-IR of adsorbed 2,6-di-tert-butylpyridine. [f] Crystallographic diameter based on atomic radii from the International Zeolite Association.[27]

The nitrogen sorption isotherm of HMASN displays a typical IV isotherm with a type-H4 hysteresis loop starting from the relative pressure $p/p_o$ at 0.4 (Fig. S4), revealing characteristics of mesopores in the shells and hollow interiors. HMASN shows a narrow pore size distribution centered at 25 Å using the BJH method. The BET surface area and pore volume of HMASN are calculated to be 1291 $cm^2 g^{-1}$ and 3.9 $cm^3 g^{-1}$, respectively (Table 1). In comparison, the pore volume of MCM-41 nanoparticle (MSN) is 2.0 $cm^3 g^{-1}$. These results indicate that the hollow nanostructures significantly enlarge the pore volumes.

The incorporation of aluminum usually creates a number of acid sites in the silica framework. The acidity of HMASN was investigated by in situ FT-IR spectroscopy of adsorbed pyridine (Py) and 2,6-di-tert-butylpyridine (DTBPy). HMASN displays an absorption band corresponding to Py interacting with Brønsted acid sites at 1545 $cm^{-1}$ (Fig. S5). The concentration of Brønsted acid sites is 59 µmol $g^{-1}$ calculated based on the Emeis equation[28] (Table 1). The acid value of HMASN probed with DTBPy yields absorption band (1530 $cm^{-1}$) up to 57 µmol $g^{-1}$. Widely used aluminum

contained MCM-41 (Al-MCM-41) and protonated ZSM-5 (HZSM-5) with similar Si/Al ratio are chosen as comparison. Although the B acid value of HMASN is smaller than HZSM-5 tested by Py, the accessible Brønsted (AB) acid value of HMASN is larger than HZSM-5 (34 µmol $g^{-1}$) tested by DTBPy. The reason is that DTBPy (kinetic diameter 10.5 Å)[29] is too large to penetrate into the 10-MR micropores of ZSM-5, and hence binds exclusively to external Brønsted acid sites. Whereas, the acid sites in mesoporous channel of HMASN are more accessible for DTBPy, i.e. big molecules.
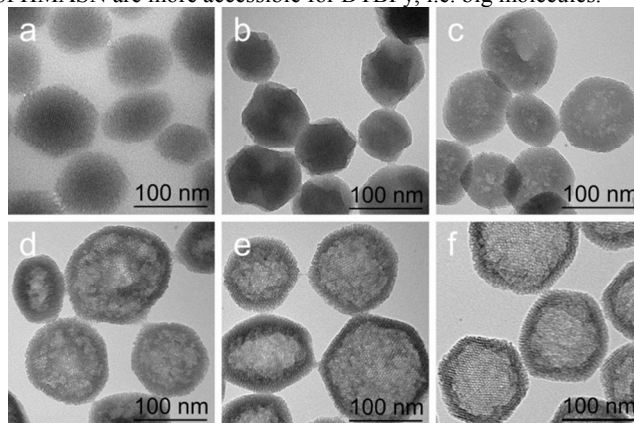


**Fig. 2** TEM images of the morphological evolution of as-prepared HMASNs. (a) Pre-made nanosized MCM-41 seeds, and aluminosilica intermediates after the Al species added for (b) 0 h, (c) 1 h, (d) 2 h, (e) 3 h, and (f) 20 h.

The evolution of hollow morphology is illustrated in Fig. 2. Fig. 2a shows the morphology of nanosized MCM-41 seeds (NMS) with an average size of 94 nm. Followed by dropping the aluminum isopropoxide $(Al(O^iPr)_3)$ ethanolic solution, the seeds are in situ coated by a light grey periphery and enlarged to approx. 100 nm as shown in Fig. 2b. The EDX line scanning analysis (Fig. S6a) reveals that the shell of the particle is rich in aluminum whereas silicon concentrates in the core. After reaction for 1 h, voids begin to develop inside the silicate cores (Fig. 2c), and the Al and Si atoms are evenly distributed in the framework as demonstrated by the EDX line scan profiles (Fig. S6b). Further prolonging the reaction time, the inner cores are completely consumed, and the central cavities are clearly distinguishable under TEM, in Fig. 2d-f. It suggests that the aluminum species are firstly condensed on the surface of the silica seeds, and then the silica is integrated with aluminates and finally migrates from center to the shells.

To study the underlying reason of the hollow cavity formation, a control experiment was performed, using tetraethyl orthosilicate (TEOS) instead of $(Al(O^iPr)_3)$ in the synthesis procedure. The result shows no voids generated during the reaction (Fig. S7). It is suggested that the Al substitution might makes the silicate framework more negative charged and results in a stronger electrostatic interaction with the cationic surfactant. Thus, Al-substituted mesoporous silica seems more stable than pure silica framework, and the less stable pure silica would dissolve and migrate to the outer layer to form aluminosilicates in the basic conditions. It can be concluded that Al heteroatom is essential to form the hollow nanostructures.

Another experiment was performed to understand the hollow cavity formation. When the silica seeds are lack of ordered mesoporous structures (Fig. S8a, b), solid aluminosilica nanoparticles are obtained after aging at 50 °C for 20 h (Fig. S8c). When the mesostructures of the silica seeds are only present in (100) plane (Fig. S8d, e), it yields the TWT hierarchical nanostructures (Fig. S8f). When the (100), (110), and (200) planes are evident in the silica seeds (Fig. S8g, h), well-defined hollow MCM-41

aluminosilica nanocages are formed after the Al induced transformation (Fig. S8i). These results suggest that ordered MCM-41 structures can accelerate the consumption of silicate cores, and facilitate the Al induced solid to hollow transformation.
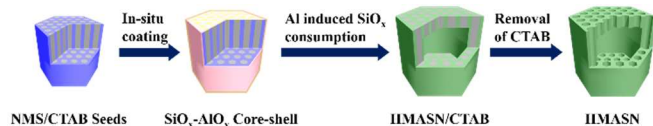


**Scheme 1** Proposed formation mechanism of HMASN.

On the basis of the above results, the formation mechanism of HMASN is proposed as illustrated in Scheme 1. Firstly, monodispersed nanosized MCM-41 silica (NMS) is chosen as seeds, and then the post-adding aluminum species are hydrolyzed and in situ coated on the surface of the seeds to form core-shell type silica-alumina intermediates with slightly enlarged sizes. Finally, the Al heteroatoms induce the consumption of silicate cores to migrate and integrate with the aluminate shells, resulting in aluminum-doped MCM-41 hollow nanostructures. The hollow MCM-41 aluminosilica nanocages (HMASN) are obtained by removing CTAB in mesopores.
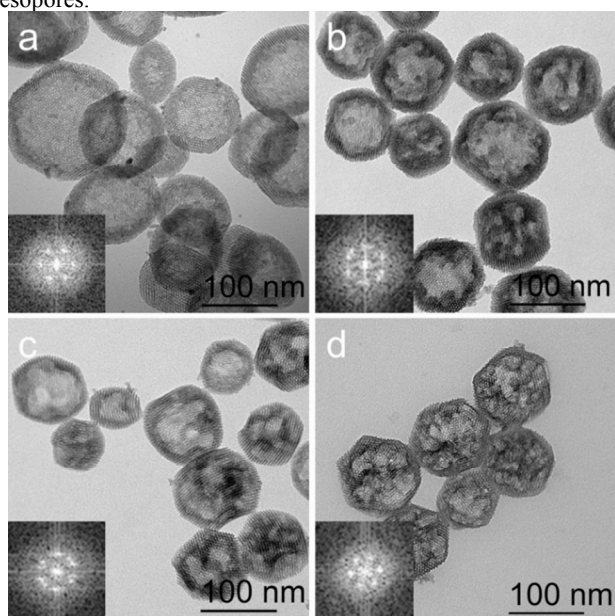


**Fig. 3** TEM images of (a) Sn, (b) Nb, (c) Fe, (d) Ti -doped hollow MCM-41 nanocages, the insets: FFT of their core parts, respectively.

Owing to the proposed formation mechanism, we successfully extended the methodology to fabricate Sn, Nb, Fe, and Ti -doped hollow MCM-41 nanocages as demonstrated in Fig. 3a-d, using the same method with precisely controlled reaction conditions (detailed in supporting information).
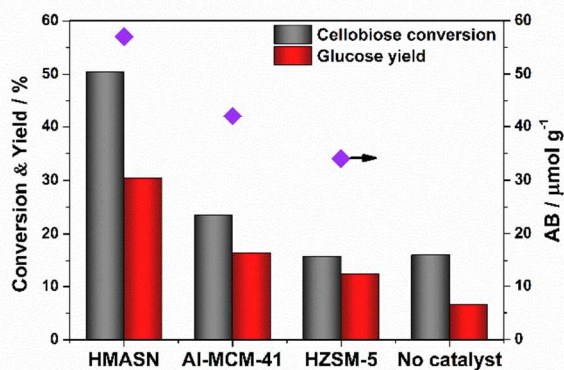


**Fig. 4** Catalytic performances of molecular sieves in cellobiose hydrolysis reaction related to their accessible Brønsted acid sites (AB). Reaction conditions: 25 mg cellobiose, 2.5 mL $H_2O$, 12.5 mg molecular sieves, 165 $^o$C, 4 h, stirring at 800 rpm.

Cellobiose consists of two glucose molecules linked by a β-(1→4) glycosidic bond which represents the typical linkage in cellulose.[30-33] Thus, hydrolysis of cellobiose (kinetic diameter 8.6 Å)[34] was chosen as model reaction. The catalytic performance of HMASN was evaluated at 165 $^o$C for 4h, compared with solid Al-MCM-41(structure information in Fig. S9) and microporous HZSM-5 zeolite. The results were shown in Fig. 4, and glucose was detected as the main product. As a control, the glucose yield is 6.7% without any catalyst. Al-MCM-41 gives a yield of 16.5% with conversion of 23.6%, and HZSM-5 affords a yield of 12.4% with conversion of 15.8%. Under same reaction conditions, HMASN achieves a yield of 30.5% with conversion of 50.5%. The enhanced activity could be attributed to that HMASN provides the open shortened mesoporous channels in the shell connecting the hollow interiors and the exteriors which form a free way around the acid sites favourable for the accessing of cellobiose and the leaving of products like glucose.

In summary, we have synthesized uniform Al, Sn, Fe, Nb and Ti -doped hollow nanocages with MCM-41 moleculear sieve structures. The average cage size is around 120 nm and shell thickness is 16 nm. The Al-doped hollow MCM-41 nanocages have stable suspensions in water, significantly improved accessible active sites, and show enhanced activity in catalytic hydrolysis of cellobiose compared with solid Al-MCM-41 and HZSM-5. The formation process provides a new strategy to generate heteroatom-doped hollow materials with ordered porous structure. The unneutral charge properties, extremely short channel length and ordered channel into the hollow interior of our materials open a new avenue in catalysis and drug delivery system.

## Acknowledgements

## Notes and references

[a] State Key Laboratory of Catalysis, Dalian Institute of Chemical Physics, Chinese Academy of Sciences, Dalian National Laboratory of Clean Energy, Dalian 116023, P. R. China. E-mail: lufang@dicp.ac.cn, xujie@dicp.ac.cn; Fax: +86-411-84379245; Tel: +86-411-84379245

[b] University of Chinese Academy of Sciences, Beijing 100049, P. R. China

1   D. Y. Zhao, J. L. Feng, Q. S. Huo, N. Melosh, G. H. Fredrickson, B. F. Chmelka and G. D. Stucky, *Science*, 1998, **279**, 548.

2   J. Y. Ying, C. P. Mehnert and M. S. Wong, *Angew. Chem. Int. Ed.*, 1999, **38**, 56.

3   J. S. Beck, J. C. Vartuli, W. J. Roth, M. E. Leonowicz, C. T. Kresge, K. D. Schmitt, C. T. W. Chu, D. H. Olson, E. W. Sheppard, S. B. Mccullen, J. B. Higgins and J. L. Schlenker, *J. Am. Chem. Soc.*, 1992, **114**, 10834.

4   C. T. Kresge, M. E. Leonowicz, W. J. Roth, J. C. Vartuli and J. S. Beck, *Nature*, 1992, **359**, 710.

5   A. Taguchi and F. Schüth, *Micropor. Mesopor. Mat.*, 2005, **77**, 1.

6   M. Vallet-Regí, F. Balas and D. Arcos, *Angew. Chem. Int. Ed.*, 2007, **46**, 7548.

7   I. Slowing, J. L. Vivero-Escoto, C. W. Wu and V. S. Y. Lin, *Adv. Drug Del. Rev.*, 2008, **60**, 1278.

8   Z. H. Luan, M. Hartmann, D. Y. Zhao, W. Z. Zhou and L. Kevan, *Chem. Mater.*, 1999, **11**, 1621.

9   A. Corma, *Chem. Rev.*, 1997, **97**, 2373.

10  Y. Wang, Q. H. Zhang, T. Shishido and K. Takehira, *J. Catal.*, 2002, **209**, 186.

11  D. R. Wang, L. Xu and P. Wu, *J. Mater. Chem. A*, 2014, **2**, 15535.

12  Z. Chen, F. Lu, J. J. Zhang, W. Q. Yu, F. Wang, J. Gao and J. Xu, *ChemCatChem*, 2013, **5**, 2822.

13  Y. S. Li and J. L. Shi, *Adv. Mater.*, 2014, **26**, 3176.

14  S. H. Wu, C. Y. Mou and H. P. Lin, *Chem. Soc. Rev.*, 2013, **42**, 3862.

15  K. Zhang, L. L. Xu, J. G. Jiang, N. Calin, K. F. Lam, S. J. Zhang, H. H. Wu, G. D. Wu, B. Albela, L. Bonneviot and P. Wu, *J. Am. Chem. Soc.*, 2013, **135**, 2427.

16  J. Liu, F. Liu, K. Gao, J. S. Wu and D. F. Xue, *J. Mater. Chem.*, 2009, **19**, 6073.

17  H. P. Lin and C. Y. Mou, *Science*, 1996, **273**, 765.

18  C. W. Wu and Y. Yamauchi, *J. Mater. Chem.*, 2012, **22**, 1251.

19  F. Lu, S. H. Wu, Y. Hung and C. Y. Mou, *Small*, 2009, **5**, 1408.

20  X. L. Fang, X. J. Zhao, W. J. Fang, C. Chen and N. F. Zheng, *Nanoscale*, 2013, **5**, 2205.

21  Z. Luo, X. W. Ding, Y. Hu, S. J. Wu, Y. Xiang, Y. F. Zeng, B. L. Zhang, H. Yan, H. C. Zhang, L. L. Zhu, J. J. Liu, J. H. Li, K. Y. Cai and Y. L. Zhao, *ACS Nano*, 2013, **7**, 10271.

22  X. L. Fang, Z. H. Liu, M. F. Hsieh, M. Chen, P. X. Liu, C. Chen and N. F. Zheng, *ACS Nano*, 2012, **6**, 4434.

23  Y. S. Li, J. L. Shi, Z. L. Hua, H. R. Chen, M. L. Ruan and D. S. Yan, *Nano Lett.*, 2003, **3**, 609.

24  X. Gu, H. X. Tao, W. Schimidt, G. Z. Lu and Y. Q. Wang, *J. Mater. Chem.*, 2012, **22**, 2473.

25  W. Y. Huang, Y. Zhu, J. P. Tang, X. Yu, X. L. Wang, D. Li and Y. M. Zhang, *J. Mater. Chem. A*, 2014, **2**, 8839.

26  R. X. Jin, Y. Yang, Y. C. Zou, X. C. Liu and Y. Xing, *Chem. Eur. J.*, 2014, **20**, 2344.

27  http://www.iza-online.org.

28  C. A. Emeis, *J. Catal.*, 1993, **141**, 347.

29  J. B. Koo, N. Jiang, S. Saravanamurugan, M. Bejblová, Z. Musilová, J. Čejka and S. E. Park, *J. Catal.*, 2010, **276**, 327.

30  A. J. Kunov-Kruse, A. Riisager, S. Saravanamurugan, R. W. Berg, S. B. Kristensen and R. Fehrmann, *Green Chem.*, 2013, **15**, 2843.

31  X. C. Zhang, Z. Zhang, F. Wang, Y. H. Wang, Q. Song and J. Xu, *J. Mol. Catal. A-Chem.*, 2013, **377**, 102.

32  D. L. An, A. H. Ye, W. P. Deng, Q. H. Zhang and Y. Wang, *Chem. Eur. J.*, 2012, **18**, 2938.

33  Vilcocq, P. C. Castilho, F. Carvalheiro and L. C. Duarte, *ChemSusChem,* 2014, **7**, 1010.

34  J. Jae, G. A. Tompsett, A. J. Foster, K. D. Hammond, S. M. Auerbach, R. F. Lobo and G. W. Huber, *J. Catal.*, 2011, **279**, 257.

RSC Advances Accepted Manuscript